Ding et al. *NPG Asia Materials* (2023) 15:37
https://doi.org/10.1038/s41427-023-00484-x

NPG Asia Materials

ARTICLE Open Access

Enhanced radiosensitivity and chemoradiation efficacy in nasopharyngeal carcinoma via a dual-targeted SPION@polymer hybrid nanosensitizer

Yuxun Ding[1,2], Xiaohui Xiao[2,3], Lu Bai[2], Bowen Yang[2], Guanghui Lin[4], Lingli Zeng[2], Lisi Xie[2], Lei Li[2], Xiaohui Duan[2], Jun Shen[2], Jianhua Zhou[4] and Yue Pan[2]

Abstract

Cisplatin-based nanoparticles show good potential in enhancing the effect of nasopharynx carcinoma (NPC) therapy but are still limited by their low radiation sensitization and poor tumor targeting ability. Herein, an ingenious design of multifunctional superparamagnetic iron oxide nanoparticle (SPION)@polymer hybrid nanosensitizer (SPHN) with enhanced radiosensitization and dual-targeting capability is described. SPHN have a core-shell structure, in which radiosensitizer superparamagnetic iron oxide particle (SPION) and cis-platinum (CDDP) are encapsulated in RGD-conjugated amphiphilic block copolymers. These unique structures endow SPHN with outstanding radiosensitization and tumor targeting abilities. When combined with X-rays, SPHN showed strong promotion of the apoptosis of CNE-1 cells in vitro. In addition, RNA-seq and KEGG enrichment analyses indicated that the PI3K-Akt and TNF signaling pathways were closely related to the molecular mechanism of SPHN in chemoradiotherapy. Furthermore, gene set enrichment analysis (GSEA) revealed that SPHN + X-rays treatment decreased translation initiation pathways and the cytoplasmic translation pathway. Through a combination of radiation and chemotherapy, SPHN can achieve remarkable inhibition of tumor growth in vivo, making this nanotechnology a general platform for the chemoradiation therapy of NPC in the future.

Introduction

Nasopharyngeal carcinoma (NPC) is an epithelial carcinoma arising from the nasopharyngeal mucosal lining[1,2]. Recently, cisplatin-based chemoradiotherapy has become a new standard of NPC treatment due to the high sensitivity of NPC to ionizing radiation and cis-platinum (CDDP)[3,4]. However, the toxicity of systemic therapy remains a pertinent issue due to the low radiosensitivity of solid tumors and the poor targeted effect of free cisplatin[5].

Although the applications of cisplatin-based nanoparticles for cancer therapy have attracted a great deal of attention[6–8], the synergistic effect of radiotherapy and chemotherapy has not been substantially improved[6]. On the one hand, the sensitization ability of cisplatin-based nanoparticles is limited at clinical doses, resulting in a high radiation dose required in clinical use[1]. On the other hand, most cisplatin-based nanoparticles targeting the tumor site heavily depend on the enhanced permeability and retention (EPR) effect[9] and some positive molecular targeting groups, such as RGD peptide[10]. To date, improving the radiation sensitization and tumor targeting efficiency of nanomedicines is still a major issue in the development of nanomedicines for NPC chemoradiotherapy.

Magnetic nanoparticles (MNPs), such as Co-, Ni-, Mn- and Fe-based nanoparticles[11,12], have attracted extensive attention, not only due to their potential radiotherapy

Correspondence: Yue Pan (panyue@mail.sysu.edu.cn)
[1]Department of Otolaryngology, Longgang E.N.T. Hospital & Shenzhen Key Laboratory of E.N.T., Institute of E.N.T., 518116 Shenzhen, Guangdong, China
[2]Guangdong Provincial Key Laboratory of Malignant Tumor Epigenetics and Gene Regulation, Guangdong-Hong Kong Joint Laboratory for RNA Medicine, Department of Radiology, Medical Research Center, Sun Yat-Sen Memorial Hospital, Sun Yat-Sen University, 510120 Guangzhou, China
Full list of author information is available at the end of the article
These authors contributed equally: Yuxun Ding, Xiaohui Xiao

© The Author(s) 2023
Open Access This article is licensed under a Creative Commons Attribution 4.0 International License, which permits use, sharing, adaptation, distribution and reproduction in any medium or format, as long as you give appropriate credit to the original author(s) and the source, provide a link to the Creative Commons license, and indicate if changes were made. The images or other third party material in this article are included in the article's Creative Commons license, unless indicated otherwise in a credit line to the material. If material is not included in the article's Creative Commons license and your intended use is not permitted by statutory regulation or exceeds the permitted use, you will need to obtain permission directly from the copyright holder. To view a copy of this license, visit http://creativecommons.org/licenses/by/4.0/.

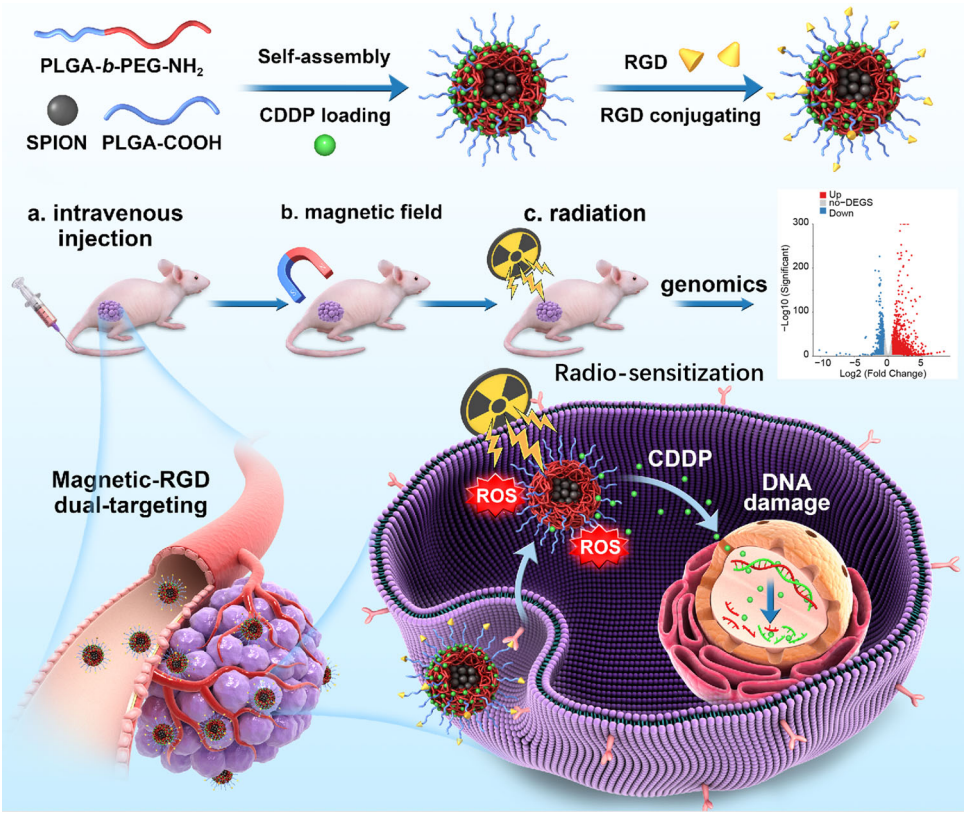

Scheme 1 Schematic representation of SPHN for effective chemoradiation therapy. The SPION was encapsulated in the hydrophobic core of SPHN using a self-assembly method, followed by coordinating CDDP with carboxyl groups on the surface of the PLGA core and conjugating RGD to the PEG shell using an amidation and click reaction. SPHN can effectively accumulate in solid tumors via a magnetic-RGD dual-targeting effect for valid CDDP delivery, resulting in a significantly improved antitumor effect with minimal side effects.

sensitization but also due to their outstanding tumor targeting properties in the presence of a magnetic field[13]. Notably, superparamagnetic iron oxide particle (SPION), one of the most commonly used magnetic nanoparticles, have been widely applied in cancer therapy[14–17]. SPION showed a good nanozyme effect for increasing the reactive oxygen species (ROS) level in the tumor microenvironment[18,19], thus improving the sensitivity of cancer cells to radiation[20–24]. Additionally, unlike molecular targeting, magnetic targeting depends on the external magnetic field rather than receptors in the tumor[25]. By precisely controlling the external magnetic field, nanomedicines can be effectively located in tumors. Therefore, the application of SPION may provide an alternative way to improve the tumor targeting efficiency of nanomedicines for effective cancer treatment, especially for tumors distributed on the mucosa or skin, such as NPC. Moreover, sufficient evidence has suggested that SPION can function as magnetic resonance (MR) contrast agents for image-guided chemoradiotherapy[26–29]. Under the guidance of imaging technology, the use of SPION would be ideal for MR-guided chemoradiotherapy of NPC.

Herein, we demonstrate dual-targeted cisplatin-based polymeric nanoparticles that can improve the overall efficacy of NPC. As illustrated in Scheme 1, the SPION@polymer hybrid nanosensitizer (SPHN) have a core-shell structure. The SPION (~5 nm) were first encapsulated inside the core with an amphiphilic block polymer, followed by conjugating CDDP to the carboxyl in the polymer and RGD in the terminus of PEG. During blood circulation, the PEGylated surface endows SPHN with long blood circulation stability. In vitro, these unique nanosensitizers showed good potential in promoting apoptosis by inducing DNA damage when combined with X-rays. In addition, RNA-seq and KEGG enrichment analysis revealed that the PI3K-Akt and TNF signaling pathways were closely related to the molecular mechanism of SPHN in chemoradiotherapy. GSEA revealed that SPHN + X-rays treatment could decrease translation initiation pathways and cytoplasmic translation pathways. Upon reaching tumor sites, the SPHN can substantially increase the tumor accumulation of CDDP in the presence of RGD and an extra magnetic field. Subsequently, the highly accumulated CDDP and SPION in the tumor

can act as chemotherapeutics and radiosensitizers for effective chemoradiotherapy. Moreover, coloading SPION can potentially provide high-resolution MR imaging for the precise therapy of NPC.

Materials and methods

Materials

Amino polyethylene glycol-block-poly(lactic-co-glycolic acid) (NH_2-PEG-*b*-PLGA), polyethylene glycol-block-poly(lactic-co-glycolic acid) (PEG-*b*-PLGA), carboxyl poly(lactic-co-glycolic acid) (PLGA-COOH) and cyclo (-RGDfC) (denoted RGD) were purchased from Guangzhou Tansh-Tech Ltd., China. SPION were purchased from Nanoeast, China.

Preparation of SPHN

For the preparation of SPHN, SPION was encapsulated in the hydrophobic PLGA core, followed by coordinating CDDP with carboxyl groups on the surface of the PLGA core and conjugating RGD in the PEG shell. Briefly, NH_2-PEG-*b*-PLGA (0.5 mg, 1 e.q.), PEG-*b*-PLGA (2 mg, 4 e.q.), PLGA-COOH (2.5 mg) and SPION (2 mg) were dispersed in 2 mL of tetrahydrofuran (THF). The solution was then added to 20 mL of phosphate buffer solution (PBS, 1 mg/mL) under vigorous stirring, followed by stirring overnight at 35 °C to remove the THF. Then, CDDP (2 mg) was added, and the mixed solution was stirred in the dark at 60 °C for 12 h. RGD was bound to PEG according to our previous work preparing SPHN[8]. Then, the SPHN solution was dialyzed against PBS for 48 h. For preparation of fluorescence-labeled nanoparticles, Cy5-NHS was employed to label the nanoparticles before RGD conjugation. Briefly, NH_2-PEG-*b*-PLGA (0.5 mg, 1 e.q.), PEG-*b*-PLGA (2 mg, 4 e.q.), PLGA-COOH (2.5 mg) and SPION (2 mg) were dispersed in 2 mL of tetrahydrofuran (THF). The solution was then added to 20 mL of phosphate buffer solution (PBS, 1 mg/mL) under vigorous stirring, followed by stirring overnight at 35 °C to remove the THF. CDDP (2 mg) was added, and the mixed solution was stirred in the dark at 60 °C for 12 h. Then, 100 μL of Cy5-NHS solution (100 μg/mL) dissolved in DMSO was added and reacted at 37 °C for 2 h. Finally, RGD was bound to PEG according to our previous work for preparing SPHN[8]. The resulting solution was dialyzed in PBS solution for 48 h.

Physicochemical characterization of SPHN

Dynamic light scattering (DLS) and zeta potential were recorded using a Malvern granulometer. Transmission electron microscopy (TEM) samples were prepared using an SPHN solution (approximately 0.05 mg/mL), and then, the morphology of the SPHN was observed via TEM. The loading efficiencies of SPION and CDDP were recorded by inductively coupled plasma mass spectrometry (ICP–MS).

In vitro stability assessment

The stability of SPHN (0.5 mg/mL) was assessed in PBS, and the dispersibility over 12 h was recorded using a camera. Then, the SPHN solution was diluted with PBS, and the diameter of the SPHN was recorded using DLS (0, 6 and 12 h).

Drug release

The release of CDDP from SPHN was determined by ICP–MS. Briefly, 1 mL of SPHN was dialyzed against 9 mL of PBS at pH 7.4, 6.5, and 5.0. Then, 1 mL of dialysate was collected at the set time for ICP–MS analysis.

In vitro reactive oxygen species (ROS) detection

Human nasopharyngeal carcinoma cells (CNE-1 cells) were plated on confocal dishes and treated with PBS, NPs/CDDP (10 μg CDDP/mL), NPs/SPION (100 μg Fe_3O_4/mL) and SPHN (10 μg CDDP/mL, 100 μg Fe_3O_4/mL). Twenty-four hours later, the cells were treated with X-rays (3 Gy), and then, the ROS level in cancer cells was tested *via* a reactive oxygen species assay kit and observed using confocal laser scanning microscopy (CLSM).

Colony formation assay

CNE-1 cells on 6-well plates were treated with SPHN (5 μg CDDP/mL) for 24 h and exposed to X-ray irradiation (3 Gy). After an additional 7 days of incubation, the colonies were fixed with 4% paraformaldehyde for 15 min. Then, the colonies were stained with 0.1% crystal violet and recorded using an AID vSpot Spectrum plate reader.

Cell apoptosis analysis

CNE-1 cells on 6-well culture plates were treated with PBS, X-rays (3 Gy), SPHN (10 μg CDDP/mL) and SPHN (10 μg CDDP/mL) + X-rays (3 Gy). After an additional 24 h incubation, all cells were collected, washed with PBS three times, stained with an Annexin V-FITC/PI apoptosis kit and then recorded *via* flow cytometry (FCM).

In vitro combined antitumor effect

The in vitro treatment effect of SPHN on CNE-1 cells was assessed *via* Cell Counting Kit-8 (CCK-8) kits. CNE-1 cells plated on 96-well plates were treated with SPHN for 12 h with different CDDP concentrations (0-50 μg/mL) and irradiated with X-rays (3 Gy). After an additional 12 h incubation, CNE-1 cells were administered 5% CCK-8 for 2 h. Then, the treatment effect was monitored using a microplate reader.

DNA damage assessment

CNE-1 cells seeded on confocal dishes were treated with SPHN (10 μg CDDP/mL) for 24 h and then irradiated with X-rays (3 Gy). Twelve hours later, the cells were fixed with 4% paraformaldehyde for 15 min, treated with 0.1% Triton

X-100 for 20 min, treated with 1% BSA for 1 h, and stained with γH2AX antibody (Alexa Fluor® 488 Mouse anti-H2AX (pS319)) at 4 °C overnight. Finally, the cells were washed with PBS three times, stained with DAPI and then imaged using CLSM.

Western blotting

CNE-1 cells seeded on 6-well culture plates were treated with PBS, X-rays, SPHN and SPHN + X-rays at a CDDP dose of 10 μg/mL and a radiation dose of 3 Gy and incubated for 24 h, washed with PBS three times, lysed with RIPA buffer solution containing phosphatase and protease inhibitors for 0.5 h, and centrifuged at 12,000 rpm at 4 °C for 0.5 h. The proteins were collected, and their concentrations were quantified by a BCA protein assay. Cell lysates were separated by SDS–PAGE, transferred to a PVDF membrane, and probed with primary antibodies. Membranes were then probed with secondary antibodies against H_2AX, γH_2AX and β-actin and imaged after enhanced chemiluminescence (ECL) reagents.

Transcriptome sequencing (RNA-Seq)

CNE-1 cells, plated in 6-well culture plates, were treated with PBS, SPHN, X-rays and SPHN + X-rays at a CDDP dose of 10 μg/mL and a radiation dose of 3 Gy. After 24 h of X-rays irradiation, cells were collected, added to 1 ml of TRIzol, and sent to Ige Biotechnology, Ltd. (Guangzhou, China), for RNA extraction and sequencing. An Illumina NovaSeq 6000 System was used for RNA-seq. Fragments per kilobase per million mapped fragments (FPKM) were utilized for gene expression level analysis.

In vivo targeting effect

The in vivo dual-targeting performance of SPHN was assessed in CNE-1 tumor-bearing mice. Groups 1 and 2 were treated with Cy5-labeled non-RGD and SPHN, respectively. Group 3 was injected with Cy5-labeled SPHN and then treated with a magnetic field for 1 h. In vivo imaging was performed in a Kodak IS in vivo FX imaging system at 12 h post-administration. Then, all mice were sacrificed to harvest major organs and tumors for ex vivo imaging. Finally, the tumors were collected to prepare 12 μm-thick paraffin sections, stained with Prussian blue and observed via an optical microscope.

In vivo chemoradiotherapy effect

BALB/c nude mice (4-5 weeks) were inoculated with CNE-1 cells. Ten days later, the mice were treated with PBS, CDDP + X-rays, SPHN, SPHN + X-rays, SPHN +magnetic field (denoted as SPHN(M)) and SPHN(M) + X-rays on Day 1, Day 3 and Day 5 at a CDDP dose of 2 mg/kg. On Days 2, 4 and 6, the CDDP + X-rays, SPHN + X-rays, and SPHN(M) + X-rays groups were treated with X-rays at an irradiation dose of 3 Gy. Tumor size and body weight were recorded for 21 days.

Immunohistochemical staining

The tumors were collected and fixed in 4% paraformaldehyde for 48 h. Then, 4 μm-thick paraffin sections were prepared for HE staining, and the cellular morphologies of tumor tissues were observed *via* an optical microscope (Leica DMI6000 B). With a similar method, HE staining of the major organs of the SPHN(M) + X-rays-treated groups was performed. Eight micrometer-thick frozen sections were prepared for TUNEL and γ-H2AX staining. After staining with 4′,6-diamidino-2-phenylindole (DAPI, blue fluorescence), the cells were observed using CLSM.

Blood biochemical tests

Blood samples from PBS- or SPHN-treated mice were harvested in heparinized Eppendorf tubes. Key indicators, including alanine transaminase (ALT), aspartate aminotransferase (AST), albumin (ALB), total bilirubin (TBIL), blood urea nitrogen (BUN), and creatinine (Crea), were detected using a fully automatic biochemical analyzer (Chemray 800, China).

In vivo magnetic resonance (MR) imaging

CNE-1 tumor-bearing nude mice were scanned using an MR scanner (Fov: 45×45, thickness: 1 mm, matrix: 224×221, slices: 12, TE: 600 ms, TR: 1200, voxel: 0.2×0.203). With the same method, the acquisition of MRI signals generated by SPHN in the tumor region was performed after SPHN treatments (50 μL, 10 μg SPION/mL).

Results

Preparation and characterization of SPHN

SPHN were prepared using a self-assembly strategy[30,31]. The morphology and structure of the SPHN were then confirmed by DLS, TEM and zeta potential analysis. As shown in Fig. 1a, the increase in particle size from 6 ± 2 nm to 80 ± 20 nm is consistent with the TEM observations (Fig. 1b), indicating the successful encapsulation of SPION in a hydrophobic PLGA core. The zeta potentials display the weak negative surface charge of SPHN under different pH conditions (pH 7.4, 6.5 and 5.0) (Fig. S1). The contents of Pt and Fe were found to be approximately 5.3% and 13.1% by ICP–MS, suggesting the successful loading of CDDP and SPION, and the loading efficiency was determined to be approximately 9.06% and 27.07%, respectively. Accordingly, the PEGylated shell coating can endow nanoparticles with improved stability. To evaluate the stability of SPHN, we first observed the in vitro dispersibility in PBS over 12 h. As depicted in Fig. S2, well-dispersed distributions were observed in the SPHN solution, even after standing for 12 h. Moreover,

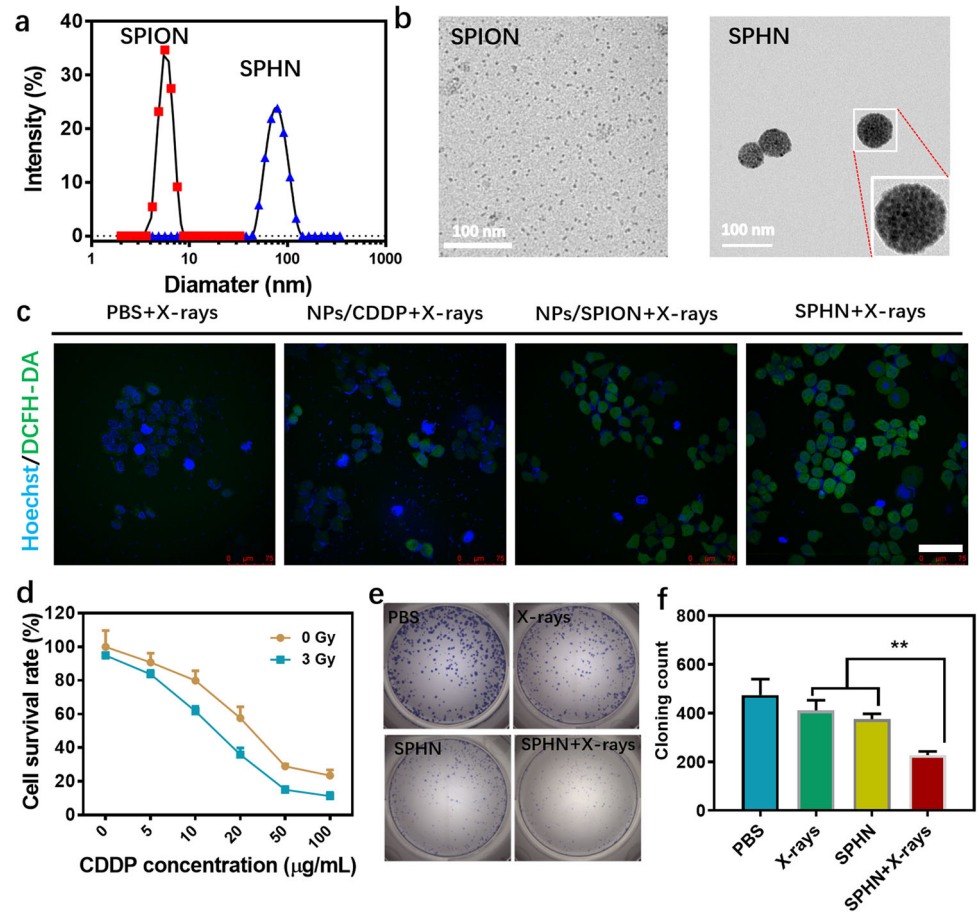

Fig. 1 Characterization of SPHN and their in vitro therapeutic effect on CNE-1 cells. a, **b** DLS histogram and TEM images of SPION and SPHN. **c** CLSM observation of the ability to produce ROS in CNE cells after treatment with PBS, NPs/CDDP (10 μg CDDP/mL), NPs/SPION (29.8 μg SPION/mL), and SPHN (10 μg CDDP/mL, 29.8 μg SPION/mL). All cells were treated with X-rays (3 Gy) 24 h later. The scale bar is 75 μm. **d** The cytotoxicity of CNE-1 cells treated with SPHN and SPHN + X-rays (3 Gy). **e**, **f** The colony formation assay (**e**) and statistical analysis (**f**) in CNE-1 cells after treatment with PBS, SPHN (10 μg CDDP/mL), X-rays (3 Gy), and SPHN (10 μg CDDP/mL)+X-rays (3 Gy). $^{**}P < 0.01$.

negligible changes in the particle size distribution and intensity were observed in the SPHN PBS solution, which confirmed the good stability of SPHN in vitro. In addition, the release of CDDP was pH-dependent and increased with decreasing pH (Fig. S3).

In vitro therapeutic effect

Accordingly, evidence suggests that CDDP has been extensively used as a radiosensitizer to enhance radiotherapy[8]. Interestingly, iron oxide nanoparticles also exhibit X-ray-induced radiosensitization effects on cancer cells. Therefore, we next investigated the ROS production ability of CNE-1 cells *via* CLSM. Compared with that of the PBS-treated group, enhanced mean fluorescence intensity appeared on the cells treated with CDDP-loaded nanoparticles (NPs/CDDP) and SPION-loaded nanoparticles (NPs/SPION). More importantly, the strongest fluorescence appeared in the SPHN-treated mice in the presence of X-rays (3 Gy), which was also verified by CLSM observations (Fig. 1c and Fig. S4), indicating that the combination of SPHN and X-rays can significantly increase the ROS content in cancer cells. Additionally, more G2/M cells were observed in the SPHN and SPHN + X-ray-treated groups (Fig. S5), revealing that our nanomedicines can achieve G2/M cell cycle arrest in CNE-1 cells. Taken together, these results suggest that the codelivery of CDDP and SPION in SPHN, by and large, can improve the radiosensitization effect for enhanced radiotherapy.

Next, we investigated the therapeutic effect of SPHN in CNE-1 cells. As shown, the survival rates of the cells cotreated with SPHN and X-rays (3 Gy) were noticeably decreased in comparison with that of the no irradiation group (SPHN, 0 Gy) (Fig. 1d and Fig. S6). After combination with X-rays, the IC50 of SPHN declined from 26.5 ± 2.9 μg CDDP/mL to 14.1 ± 1.9 μg CDDP/mL

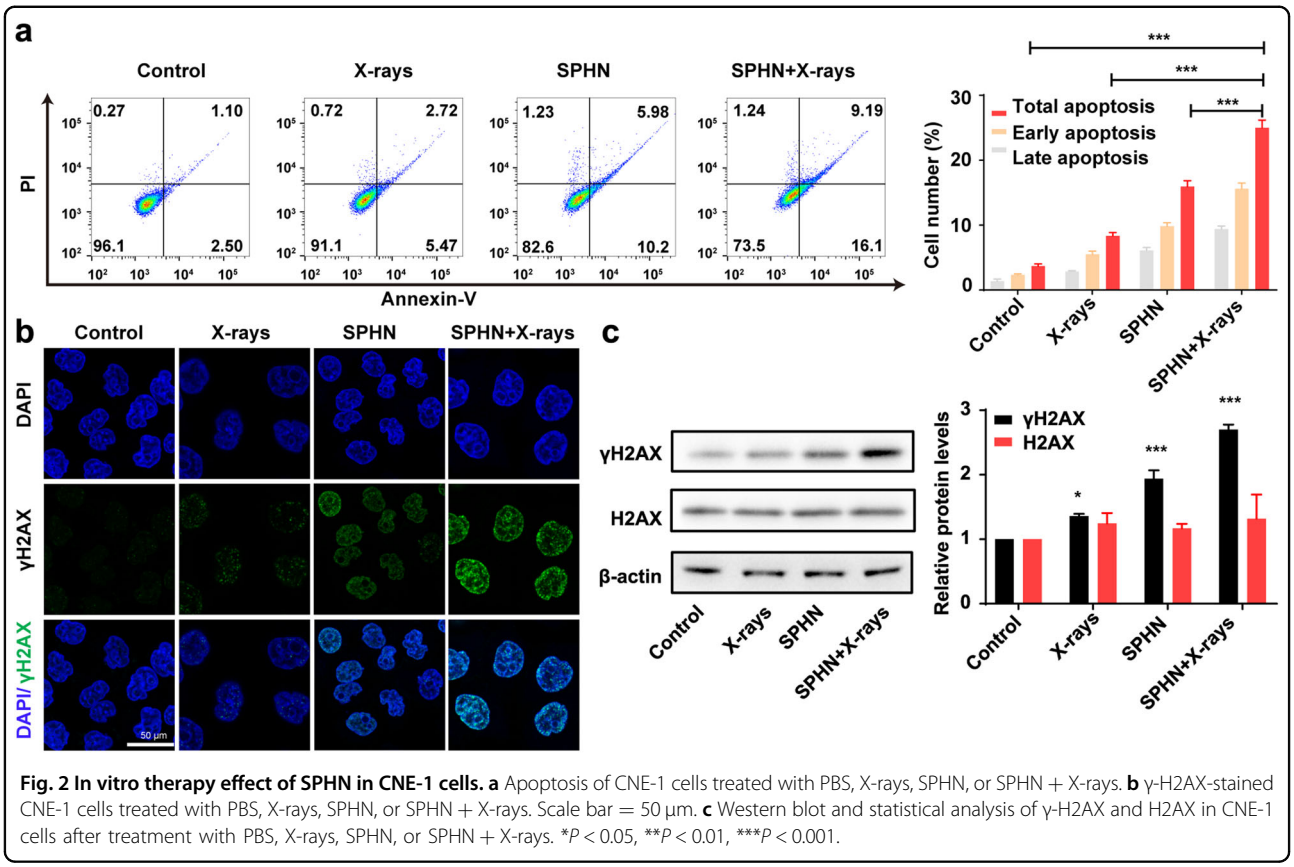

Fig. 2 In vitro therapy effect of SPHN in CNE-1 cells. a Apoptosis of CNE-1 cells treated with PBS, X-rays, SPHN, or SPHN + X-rays. **b** γ-H2AX-stained CNE-1 cells treated with PBS, X-rays, SPHN, or SPHN + X-rays. Scale bar = 50 μm. **c** Western blot and statistical analysis of γ-H2AX and H2AX in CNE-1 cells after treatment with PBS, X-rays, SPHN, or SPHN + X-rays. *$P < 0.05$, **$P < 0.01$, ***$P < 0.001$.

(Fig. S7), which suggested that X-ray irradiation can improve the therapeutic effect. To further investigate the potential of SPHN for combined chemoradiation therapy, we evaluated the combined effect using a colony formation experiment. The results indicated that the cell proliferation rate was lower in the SPHN + X-ray-treated cells than in the cells treated with SPHN or radiation alone, confirming that this chemoradiotherapy strategy can significantly inhibit the proliferation of CNE-1 cells (Fig. 1e, f).

Moreover, analysis of cell apoptosis was used to determine the early and late apoptotic cells in CNE-1 cells administered different formulations (Fig. 2a). The percentage of apoptotic cells was 25.29% after SPHN + X-rays treatment and markedly increased compared to that of SPHN or X-rays alone, which were 16.18% and 8.19%, respectively, suggesting that the combination of SPHN and irradiation can accelerate the apoptosis of CNE-1 cells, thus improving the therapeutic effect. To further investigate the antitumor mechanism of SPHN and X-rays, we next observed γ-H2AX, a representative DNA damage marker, by CLSM. As shown in Fig. 2b, the strongest green fluorescence was observed in the cell nucleus of CNE-1 cells treated with SPHN + X-rays. The western blot results also revealed the highest level of γ-H2AX under the combined action of SPHN and X-rays (Fig. 2c), suggesting that the combination of SPHN and X-rays can induce the highest DNA damage and thus improve the anticancer activity for NPC therapy.

RNA-seq analysis

To determine the cytotoxic mechanisms of SPHN and X-rays, we performed RNA-seq on CNE-1 cells treated with SPHN and X-rays. Venn diagrams visualize the number of common and differentially expressed genes between groups of combinations (Fig. S8). Compared with those of the control group, 332 genes were upregulated (red dots) and 229 genes were downregulated in the X-ray group (Fig. S9a); however, 2513 genes were upregulated and 1137 genes were downregulated in the SPHN group (Fig. S9b). Compared with those of the control group, 2667 genes were upregulated and 1422 genes were downregulated in the SPHN + X-ray group (Fig. 3a). Kyoto Encyclopedia of Genes and Genomes (KEGG) enrichment analysis showed that the genes involved in the tumor necrosis factor (TNF), PI3K-Akt, extracellular matrix (ECM) receptor interaction, NF-kappa B and JAK-STAT pathways were significantly affected by SPHN + X-ray treatment (Fig. 3b). Gene set enrichment analysis (GSEA) was used to further verify the therapeutic mechanism of SPHN in chemoradiotherapy. We performed GSEA based on the Gene Ontology (GO)

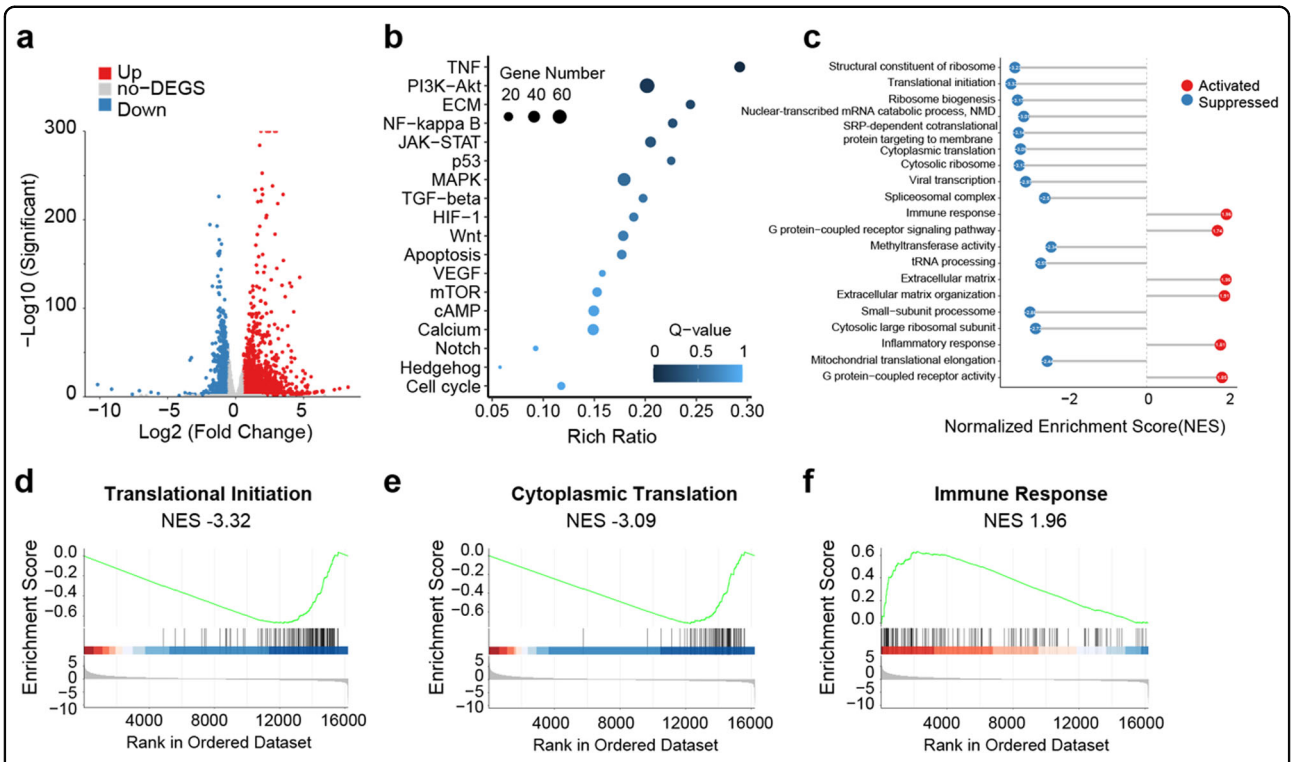

Fig. 3 The RNA-seq analysis on CNE-1 cells. a The differentially expressed gene volcano plot comparing the SPHN + X-rays group vs. the control group. Log2 (fold change): log2 value of the fold of difference; Up: upregulated genes, Down: downregulated genes; no-DEGS (no differentially expressed genes): genes with no significant difference. **b** Bubble chart of KEGG enrichment analysis between the SPHN + X-rays group and the control group. **c** Lollipop chart of gene set enrichment analysis (GSEA) of the regulated gene pathways with the GO database. **d**–**f** Normalized enrichment score (NES) and enrichment map of GSEA plots of differentially expressed pathways in the SPHN + X-rays treatment vs. the nontreated control.

database, and the top 20 most regulated pathways in the GSEA are shown in Fig. 3c. From the GSEA-GO lollipop chart, several transcriptional and translational signaling pathways were significantly decreased (Fig. 3c). Specifically, translation initiation pathways and cytoplasmic translation pathways were inhibited in the SPHN + X-rays group (Fig. 3d, e). In contrast, immune response pathways were activated after SPHN + X-rays treatment (Fig. 3f). These results demonstrated that SPHN + X-rays treatment might decrease the intracellular translation signaling pathway and thereby trigger apoptosis of cancer cells. Furthermore, the enhancement of the immune response pathway suggested that our therapy may lead to an immune response that further reduces the possibility of tumor recurrence.

In vivo dual targeted effect

To investigate the potential of SPHN for in vivo chemoradiotherapy, we first investigated the targeted effect of SPHN in CNE-1-bearing mice via a biodistribution experiment after administration of non-RGD nanoparticles (denoted NPs) (Fig. 4a(i)), SPHN (Fig. 4a(ii)), and SPHN combined with a magnetic field (denoted SPHN(M) (Fig. 4a(iii)). As shown in Fig. 4b, the strongest fluorescence signal was observed in the mice treated with SPHN(M), and the second strongest fluorescence appeared in the SPHN-treated group, while the weakest signal was displayed in the NP-treated mice. Additionally, consistent results were observed in the ex vivo imaging (Fig. 4c and Fig. S10) and Prussian blue staining experiments (Fig. 4d). These results revealed that RGD in the SPHN, to some extent, can improve the tumor accumulation effect of nanomedicines. After combination with the magnetic targeting of SPION, the targeted effect of SPHN would be significantly enhanced, thus providing an alternative strategy to achieve effective targeted delivery.

In vivo therapeutic effect

Next, the antitumor efficacy of SPHN was evaluated in CNE-1-bearing nude mice (Fig. 5a). Figure 5b-c shows that the mice treated with SPHN + X-rays exhibited significant tumor suppression, with a tumor inhibition rate of 86.17% versus that of PBS treatment over 21 days; this rate was significantly higher than that of the X-ray

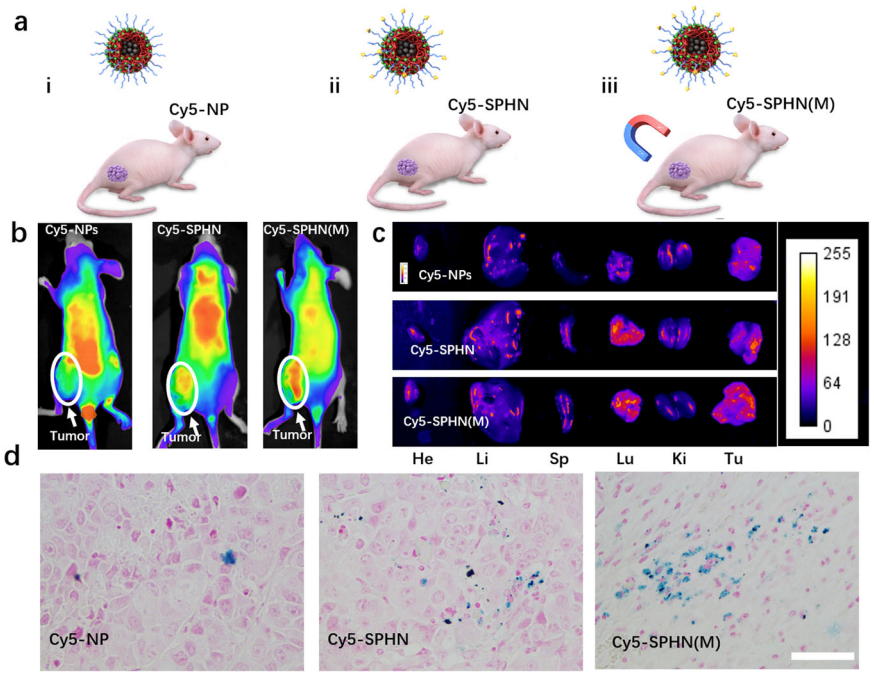

Fig. 4 The in vivo targeted effect in CNE-1-bearing mice. a A scheme showing the treatment of tumor-bearing mice. **b**, **c** Fluorescence imaging of CNE-1-bearing mice (**b**) and ex vivo organs (including heart (He), liver (Li), spleen (Sp), lung (Lu), kidney (Ki), and tumor (Tu)) from CNE-1-bearing mice that were treated with Cy5-NPs, Cy5-SPHN and Cy5-SPHN(M) for 12 h (**c**). **d** Images (100×) of Prussian blue staining of tumors from CNE-1-bearing mice treated with Cy5-NPs, Cy5-SPHN and Cy5-SPHN(M) for 12 h.

(49.99%)- and SPHN (75.46%)-treated groups. More importantly, the best tumor suppression with an inhibition rate of 94.49% was found in the SPHN(M) + X-ray-treated group due to the improved tumor accumulation resulting from the magnetic targeting of SPHN. To further demonstrate the chemoradiotherapy effect of SPHN, we conducted H&E and TUNEL staining to evaluate cell apoptosis, and γ-H2AX immunofluorescence staining was conducted to evaluate the DNA damage level. The results displayed the highest level of cell apoptosis in the tumor site and DNA damage in cancer cells after simultaneous administration of SPHN(M) + X-rays (Fig. 5d), which can also be confirmed by further statistical analysis (Fig. 5e, f), suggesting that SPHN + X-rays had the best therapeutic effect compared to other formulations.

Biosafety assessment and MRI

Biosafety is a key determinant in the in vivo application of nanomedicine. To verify the in vivo application potential of SPHN for NPC combined with chemoradiation therapy, we evaluated the biosafety of SPHN by blood biochemistry 21 days post-treatment. According to the results (Fig. 6a–f), the major indicators of liver and kidney function in the mice that were treated with SPHN were within normal limits and showed no significant differences compared to those of the mice treated with PBS. Moreover, the H&E-stained organs of the SPHN + X-ray-treated mice, including the heart, liver, spleen, lung, and kidney, exhibited no obvious histopathological abnormalities, revealing no apparent toxicities caused by SPHN in vivo (Fig. 6g). Image technology is another key determinant for cancer therapy, especially for radiotherapy or chemoradiotherapy. The SPHN are composed of SPION, a widely used MRI contrast agent, and thus show good MRI ability. To investigate the application potential of SPHN in precise NPC treatment, we assessed the in vivo MRI capability of SPHN in CNE-1 tumor-bearing mice. Compared to that of the untreated mice, an obvious T2 signal was observed on the tumors of the SPHN-treated mice (Fig. S11), suggesting that SPHN are likely to act as an MR contrast agent for MR-guided NPC chemoradiation therapy.

Discussion

Nanoparticle-based strategies for NPC chemoradiation therapy have attracted increased attention, but there has been no dramatic improvement in clinical outcomes to date, which is mainly attributed to the poor in vivo targeting ability of traditional nanomedicines. To overcome the challenges mentioned above, we developed SPHN as nanosensitizers for NPC targeted therapy. On the one hand, such nanosensitizers can significantly improve the radiotherapy effect by the radiosensitization of CDDP and SPION. On the other hand, the dual-targeted strategy can

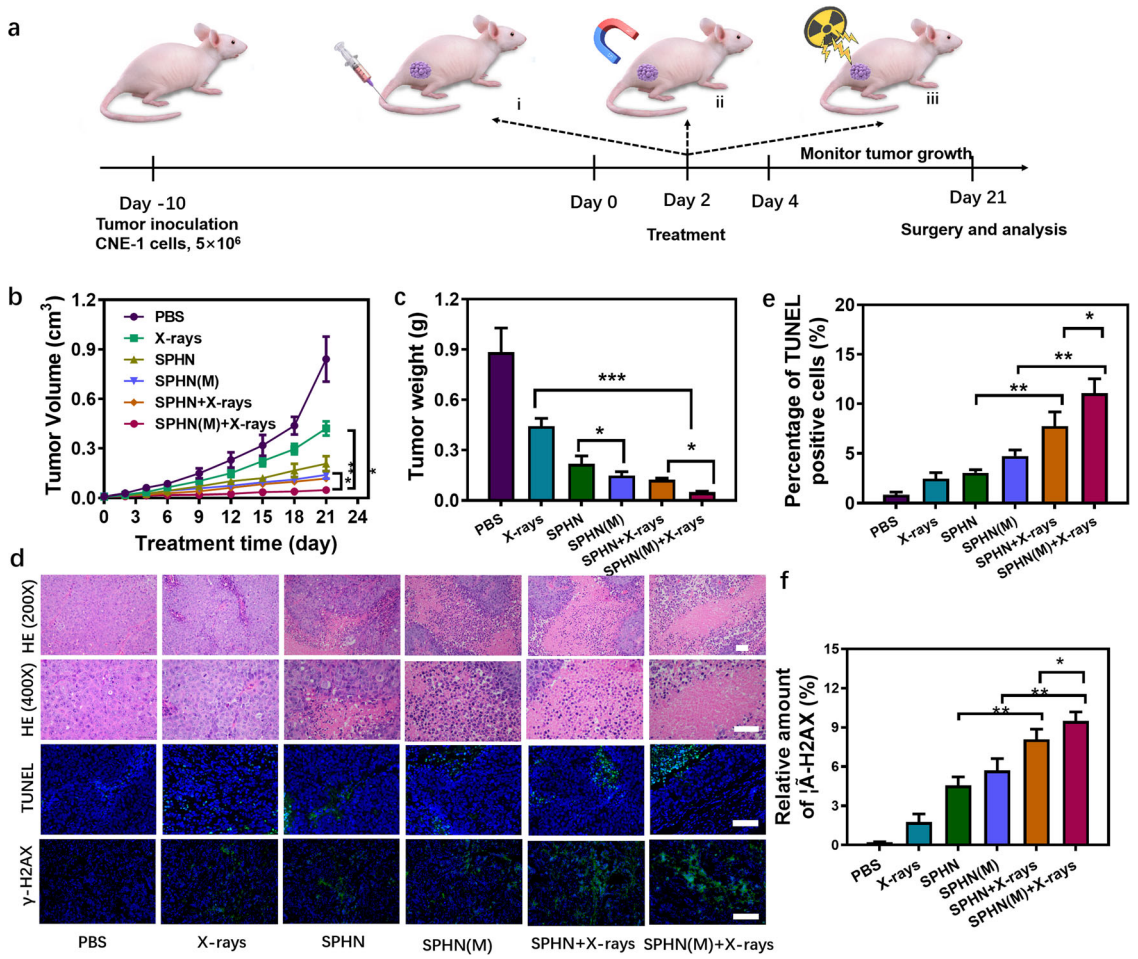

Fig. 5 The in vivo therapeutic effect in CNE-1-bearing mice. a Workflow of the in vivo experiment. **i** Intravenous injection with SPHN. **ii** Magnetic targeting. **iii** Radiation with X-rays. **b**, **c** The tumor volume growth curves (**b**) and tumor weight (**c**) in the mice treated with PBS, X-rays, SPHN, SPHN + X-rays, SPHN(M), and SPHN(M) + X-rays 3 times over 21 days. **d** Images of HE-, TUNEL- and γ-H2AX-stained tumor slices from CNE-1-bearing mice treated with PBS, X-rays, SPHN, SPHN + X-rays, SPHN(M) and SPHN(M) + X-rays. The scale bar is 100 μm. **e**, **f** Quantitative analysis of the TUNEL-positive cells (**e**) and γ-H2AX density (**f**) in the tumor tissues after treatment with PBS, X-rays, SPHN, SPHN + X-rays, SPHN(M), and SPHN(M) + X-rays. $^{*}P < 0.05$, $^{**}P < 0.01$, $^{***}P < 0.001$.

significantly improve the tumor-targeting effect of SPHN, thus achieving effective chemoradiotherapy in vivo.

Since the SPHN consist of CDDP and SPION, both of which exhibit X-ray-induced radiosensitization effects for enhancing radiotherapy, we investigated the ROS production ability of SPHN in CNE-1 cells. In Fig. 2a, the results of CLSM and FCM observation suggested that the codelivery of CDDP and SPION in SPHN, by and large, can achieve effective radiosensitization. Next, we investigated the therapeutic effect of SPHN in CNE-1 cells. With the help of X-rays, the SPHN achieved an enhanced therapeutic effect and significantly inhibited the proliferation of CNE-1 cells in vitro. In addition, the results of γ-H2AX staining revealed that the combination of SPHN and X-rays can dramatically induce DNA damage in CNE-1 cells. Altogether, our data suggest that SPHN can achieve an enhanced therapeutic effect in vitro, which is attributed to their good chemoradiation therapy.

The tumor-targeted effect plays an important role in the in vivo application of anticancer nanoagents. As shown in Fig. 4, the RGD-magnetic dual targeting design endows SPHN with outstanding tumor targeting ability. Under a magnetic field, SPHN can significantly accumulate in tumor tissue for effective targeted delivery of antitumor agents. Next, the antitumor effect of SPHN was assessed in CNE-1-bearing nude mice. As shown in Fig. 5, the mice treated with SPHN, X-rays and magnetic fields exhibited the most significant suppression of tumor growth and the highest levels of tumor apoptosis and DNA damage. Since the magnetic field can further improve the tumor accumulation of SPHN, the SPHN can achieve the most effective delivery for CDDP and SPION. In the presence

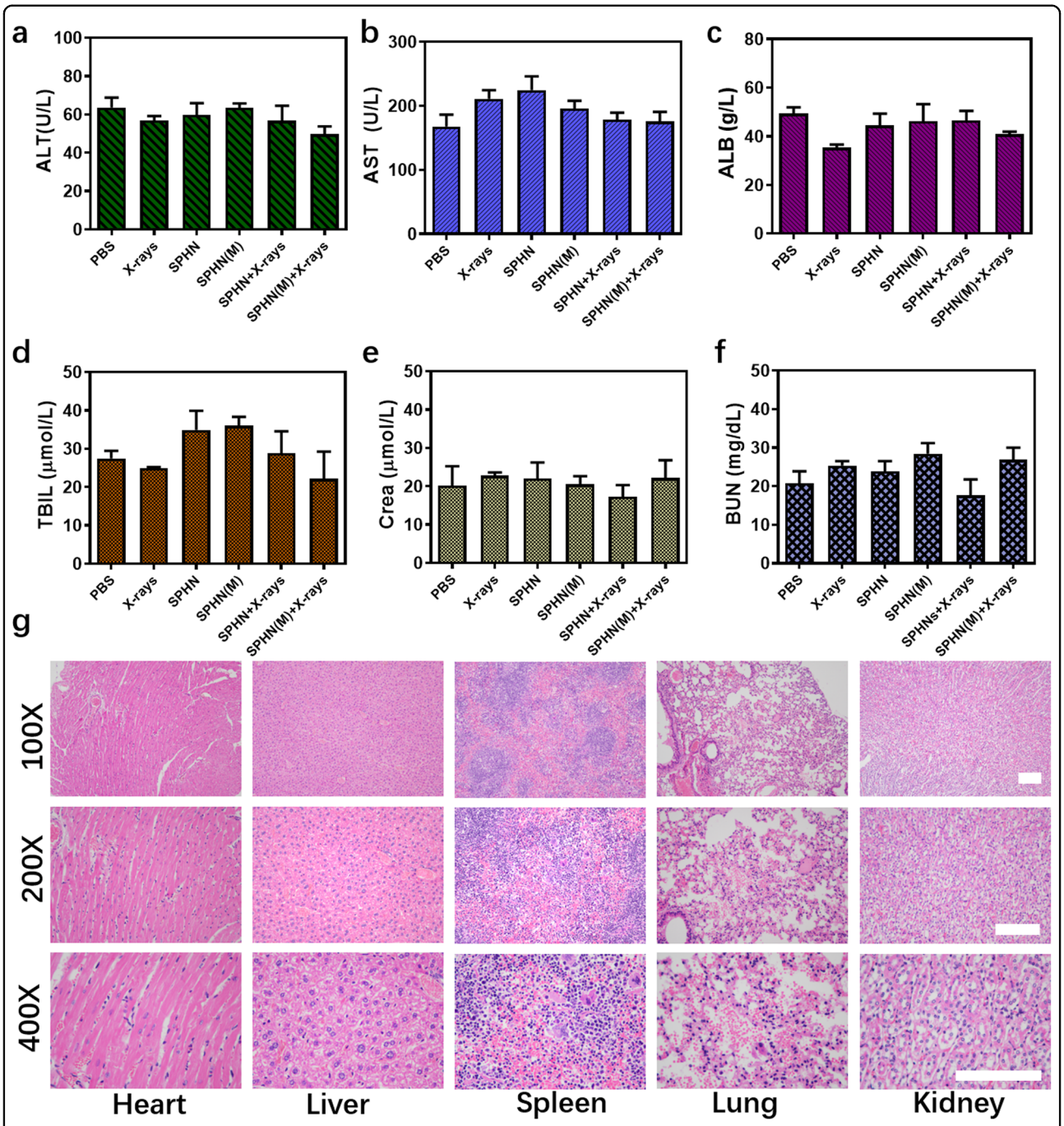

Fig. 6 Biosafety assessment of SPHN. a–f The major indicators of liver and kidney function in the mice treated with PBS, X-rays, SPHN, SPHN + X-rays, SPHN(M) and SPHN(M) + X-rays for 21 days. **g** Images of H&E-stained major organs in the SPHN(M) + X-ray treated mice 3 times over 21 days. Scale bar = 200 μm.

of X-rays, the highest accumulation of CDDP and SPION can induce the best therapeutic effect, thus achieving effective chemoradiotherapy for NPC. In addition, biosafety and therapeutic accuracy are other important factors for nanoparticle-based precise treatment. Here, the in vivo biosafety safety of SPHN was evaluated by blood biochemistry and HE staining of major organs. According to the results (Fig. 6), the indicators of liver and kidney function and the cell morphology of organs were normal after treatment with SPHN, revealing no apparent toxicities caused by SPHN in vivo. Moreover, the in vivo MRI results indicated that SPHN showed good MRI capability

(Fig. S11). Altogether, SPHN are likely to achieve a precise therapy for NPC, with no notable side effects.

Conclusion

In summary, we have developed SPHN that can effectively target tumors. With the codelivery of CDDP and SPION, SPHN can induce high-level DNA damage *via* combined chemoradiotherapy, thus inducing effective apoptosis in CNE-1 cells and significantly inhibiting their proliferation. More importantly, RGD magnetic targeting can endow SPHN with available tumor accumulation for the targeted delivery of antitumor agents in vivo, resulting in a significantly enhanced antitumor effect in CNE-1-bearing mice. Considering their potential in precise treatment, such nanoparticles may also act as an MR contrast agent for MR-guided NPC chemoradiation therapy.

Acknowledgements

We acknowledge financial support from the National Natural Science Foundation of China (82171997, U1801681, 82171996, 82103680), the Guangdong Basic and Applied Basic Research Foundation for Distinguished Young Scholars (2020B1515020027), a grant from the Guangzhou Science and Technology Bureau (202002020070, 202102010181, 202102010007), the Guangdong Science and Technology Department (2020B1212060018, 2020B1212030004), the Key R&D Program of Guangdong Province (2022B0303020001), the Shenzhen Key Medical Discipline Construction Fund (SZXK039), the Guangdong Basic and Applied Basic Research Fund Foundation (2019A1515110204, 2020A1515010523), the Yat-sen Scientific Research Project (YXQH202018), the Shenzhen Innovation of Science and Technology Commission (LGKCYLWS2020089), and the Shenzhen Science and Technology Program (JCYJ20190807160401657).

Author details

[1]Department of Otolaryngology, Longgang E.N.T. Hospital & Shenzhen Key Laboratory of E.N.T., Institute of E.N.T., 518116 Shenzhen, Guangdong, China. [2]Guangdong Provincial Key Laboratory of Malignant Tumor Epigenetics and Gene Regulation, Guangdong-Hong Kong Joint Laboratory for RNA Medicine, Department of Radiology, Medical Research Center, Sun Yat-Sen Memorial Hospital, Sun Yat-Sen University, 510120 Guangzhou, China. [3]Department of Hematology, The Seventh Affiliated Hospital, Sun Yat-sen University, 518107 Shenzhen, China. [4]School of Biomedical Engineering, Shenzhen Campus of Sun Yat-sen University, 518107 Shenzhen, China

Author contributions

Y.D. and X.X. contributed equally, carried out the experimental work and wrote the manuscript. Y.P. designed the project, supervised the study and participated in the writing-review of manuscript. L.B. and G.L. participated in the synthesis and characterization of the nanoparticles. X.D. and J.S. participated in the MRI of SPHN. B.Y., L.X., and L.L. participated in the analysis of animal results. All authors discussed the results and commented on the manuscript.

Conflict of interest

The authors declare no competing interests.

Publisher's note

Springer Nature remains neutral with regard to jurisdictional claims in published maps and institutional affiliations.

Supplementary information The online version contains supplementary material available at https://doi.org/10.1038/s41427-023-00484-x.

Received: 13 November 2022 Revised: 24 April 2023 Accepted: 26 April 2023.
Published online: 23 June 2023

References

1. Chen, Y. P. et al. Nasopharyngeal carcinoma. *Lancet* **394**, 64–80 (2019).
2. Chua, M. L. K., Wee, J. T. S., Hui, E. P. & Chan, A. T. C. Nasopharyngeal carcinoma. *Lancet* **387**, 1012–1024 (2016).
3. Blanchard, P. et al. Chemotherapy and radiotherapy in nasopharyngeal carcinoma: an update of the MAC-NPC meta-analysis. *Lancet Oncol.* **16**, 645–655 (2015).
4. Chen, Y. P. et al. Chemotherapy in combination with radiotherapy for definitive-intent treatment of stage II-IVA nasopharyngeal carcinoma: CSCO and ASCO guideline. *J. Clin. Oncol.* **39**, 840–859 (2021).
5. Chen, L. et al. Concurrent chemoradiotherapy plus adjuvant chemotherapy versus concurrent chemoradiotherapy alone in patients with locoregionally advanced nasopharyngeal carcinoma: a phase 3 multicentre randomised controlled trial. *Lancet Oncol.* **13**, 163–171 (2012).
6. Shi, J., Kantoff, P. W., Wooster, R. & Farokhzad, O. C. Cancer nanomedicine: progress, challenges and opportunities. *Nat. Rev. Cancer* **17**, 20–37 (2017).
7. Sun, Y. et al. Induction chemotherapy plus concurrent chemoradiotherapy versus concurrent chemoradiotherapy alone in locoregionally advanced nasopharyngeal carcinoma: a phase 3, multicentre, randomised controlled trial. *Lancet Oncol.* **17**, 1509–1520 (2016).
8. Ding, Y. et al. Platinum-crosslinking polymeric nanoparticle for synergetic chemoradiotherapy of nasopharyngeal carcinoma. *Bioact. Mater.* **6**, 4707–4716 (2021).
9. Ding, Y. et al. Investigating the EPR effect of nanomedicines in human renal tumors via ex vivo perfusion strategy. *Nano Today* **35**, 100970 (2020).
10. Xiao, X. et al. Self-targeting platinum (IV) amphiphilic prodrug nano-assembly as radiosensitizer for synergistic and safe chemoradiotherapy of hepatocellular carcinoma. *Biomaterials* **289**, 121793 (2022).
11. Song, G. et al. Carbon-coated FeCo nanoparticles as sensitive magnetic-particle-imaging tracers with photothermal and magnetothermal properties. *Nat. Biomed. Eng.* **4**, 325–334 (2020).
12. Xiao, Y. & Du, J. Superparamagnetic nanoparticles for biomedical applications. *J. Mater. Chem. B* **8**, 354–367 (2020).
13. Pan, Y., Du, X., Zhao, F. & Xu, B. Magnetic nanoparticles for the manipulation of proteins and cells. *Chem. Soc. Rev.* **41**, 2912–2942 (2012).
14. Xu, C. & Sun, S. New forms of superparamagnetic nanoparticles for biomedical applications. *Adv. Drug Deliv. Rev.* **65**, 732–743 (2013).
15. Gao, J., Gu, H. & Xu, B. Multifunctional magnetic nanoparticles: design, synthesis, and biomedical applications. *Acc. Chem. Res.* **42**, 1097–1107 (2009).
16. Hu, Y., Mignani, S., Majoral, J. P., Shen, M. & Shi, X. Construction of iron oxide nanoparticle-based hybrid platforms for tumor imaging and therapy. *Chem. Soc. Rev.* **47**, 1874–1900 (2018).
17. Tian, X. et al. Functional magnetic hybrid nanomaterials for biomedical diagnosis and treatment. *Wiley Interdiscip. Rev. Nanomed. Nanobiotechnol.* **10**, e1476 (2018).
18. Song, G., Cheng, L., Chao, Y., Yang, K. & Liu, Z. Emerging nanotechnology and advanced materials for cancer radiation therapy. *Adv. Mater.* **29**, 1700996 (2017).
19. Wu, J. et al. Nanomaterials with enzyme-like characteristics (nanozymes): next-generation artificial enzymes (II). *Chem. Soc. Rev.* **48**, 1004–1076 (2019).
20. Deng, Y. et al. Facile preparation of hybrid core-shell nanorods for photothermal and radiation combined therapy. *Nanoscale* **8**, 3895–3899 (2016).
21. Chen, Q. et al. Nanoparticle-enhanced radiotherapy to trigger robust cancer immunotherapy. *Adv. Mater.* **31**, 1802228 (2019).
22. Huang, G. et al. Superparamagnetic iron oxide nanoparticles: amplifying ROS stress to improve anticancer drug efficacy. *Theranostics* **3**, 116–126 (2013).
23. Wei, H. & Wang, E. Nanomaterials with enzyme-like characteristics (nanozymes): next-generation artificial enzymes. *Chem. Soc. Rev.* **42**, 6060–6093 (2013).
24. Hauser, A. K. et al. Targeted iron oxide nanoparticles for the enhancement of radiation therapy. *Biomaterials* **105**, 127–135 (2016).
25. Ding, Z. et al. Furin-controlled Fe_3O_4 nanoparticle aggregation and ^{19}F signal "turn-on" for precise MR imaging of tumors. *Adv. Funct. Mater.* **29**, 1903860 (2019).
26. Zhu, J. et al. Facile synthesis of magnetic core-shell nanocomposites for MRI and CT bimodal imaging. *J. Mater. Chem. B* **3**, 6905–6910 (2015).

27. Ding, Y., Zeng, L., Xiao, X., Chen, T. & Pan, Y. Multifunctional magnetic nanoagents for bioimaging and therapy. *ACS Appl. Bio Mater.* **4**, 1066–1076 (2021).
28. Du, X., Zhou, J., Shi, J. & Xu, B. Supramolecular hydrogelators and hydrogels: from soft matter to molecular biomaterials. *Chem. Rev.* **115**, 13165–13307 (2015).
29. Kim, D., Kim, J., Park, Y. I., Lee, N. & Hyeon, T. Recent development of inorganic nanoparticles for biomedical imaging. *ACS Cent. Sci.* **4**, 324–336 (2018).
30. Shi, J., Votruba, A., Farokhzad, O. & Langer, R. Nanotechnology in drug delivery and tissue engineering: from discovery to applications. *Nano Lett.* **10**, 3223–3230 (2010).
31. Li, X. et al. Mimetic heat shock protein mediated immune process to enhance cancer immunotherapy. *Nano Lett.* **20**, 4454–4463 (2020).